J Neurophysiol 125: 1612–1623, 2021.
First published March 3, 2021; doi:10.1152/jn.00464.2020

american physiological society

JNP JOURNAL OF NEUROPHYSIOLOGY

RESEARCH ARTICLE

Neural Circuits

Changes in pairwise correlations during running reshape global network state in the main olfactory bulb

Udaysankar Chockanathan,[1,2*] Emily J. W. Crosier,[2*] Spencer Waddle,[3] Edward Lyman,[3] Richard C. Gerkin,[4] and Krishnan Padmanabhan[1,2,5]

[1]*Medical Scientist Training Program (MSTP), University of Rochester School of Medicine, Rochester, New York;* [2]*Department of Neuroscience and Neuroscience Graduate Program (NGP), University of Rochester School of Medicine, Rochester, New York;* [3]*Department of Physics, University of Delaware, Newark, Delaware;* [4]*School of Life Sciences, Arizona State University, Tempe, Arizona; and* [5]*Center for Visual Sciences, University of Rochester School of Medicine, Rochester, New York*

Abstract

Neural codes for sensory inputs have been hypothesized to reside in a broader space defined by ongoing patterns of spontaneous activity. To understand the structure of this spontaneous activity in the olfactory system, we performed high-density recordings of neural populations in the main olfactory bulb of awake mice. We observed changes in pairwise correlations of spontaneous activity between mitral and tufted (M/T) cells when animals were running, which resulted in an increase in the entropy of the population. Surprisingly, pairwise maximum entropy models that described the population activity using only assumptions about the firing rates and correlations of neurons were better at predicting the global structure of activity when animals were stationary as compared to when they were running, implying that higher order (3rd, 4th order) interactions governed population activity during locomotion. Taken together, we found that locomotion alters the functional interactions that shape spontaneous population activity at the earliest stages of olfactory processing, one synapse away from the sensory receptors in the nasal epithelium. These data suggest that the coding space available for sensory representations responds adaptively to the animal's behavioral state.

NEW & NOTEWORTHY The organization and structure of spontaneous population activity in the olfactory system places constraints of how odor information is represented. Using high-density electrophysiological recordings of mitral and tufted cells, we found that running increases the dimensionality of spontaneous activity, implicating higher order interactions among neurons during locomotion. Behavior, thus, flexibly alters neuronal activity at the earliest stages of sensory processing.

locomotion; maximum entropy; mitral/tufted cells; olfactory bulb; population coding

INTRODUCTION

Behavioral states, such as quiescence and wakefulness (1), locomotion (2, 3), and arousal (4), can have marked effects on patterns of neuronal activity throughout the brain. In sensory systems, neural activity can change in response to these behaviors, even in the absence of any sensory stimuli. This spontaneous activity often reflects the underlying organization of the circuit (5, 6), constraining what types of activity patterns are possible for encoding sensory stimuli (7). These latent behavioral states consequently shape the variability of neuronal responses in primary sensory areas (8)

As in the neocortex, neural activity in the main olfactory bulb is strongly influenced by behavioral state (9). The principal neurons of the main olfactory bulb, the mitral and tufted cells (M/T), receive direct input from the olfactory receptor neurons (ORNs) in the nasal epithelium, process these initial odor responses via connections with one another and with local inhibitory interneurons, and relay this information to downstream cortical areas (10). Spontaneous firing rates in the principal M/T cells are lower under anesthesia as compared with waking (11). M/T cell firing can also be altered based on experience and training (12–14), on reward (15), and can indicate nonolfactory information such as behavioral

* U. Chockanathan and E. J. W. Crosier contributed equally to this work.
Correspondence: K. Padmanabhan (Krishnan_padmanabhan@urmc.rochester.edu).
Submitted 5 August 2020 / Revised 1 March 2021 / Accepted 1 March 2021

choice (16, 17). Although the behavioral modulation of M/T activity is not surprising, given the link between olfaction, sniffing, and whisking (18–23), the fact that such modulation occurs in principal cells one synapse away from the sensory periphery (10, 24), suggests that behavior impacts neuronal coding earlier in olfactory processing (25) as compared with other sensory systems in mammals. Centrifugal projections into the bulb (26–29) from a diversity of areas including the hippocampus (30, 31), point to a diversity of anatomical connections that link olfactory processing in the bulb to complex behaviors (32) including running. Although a number of recent studies suggest that locomotion and running exert substantial influence on population activity in sensory neocortices (2, 3, 8, 33), it is less clear how locomotion, which is essential for a number of olfactory behaviors including foraging (34) and tracking (35), influences the activity of ensembles of neurons in the earliest stages of olfactory coding.

To address this, we recorded simultaneously from hundreds of M/T cells in the main olfactory bulb (MOB) while head-fixed animals ran on a cylindrical wheel. Not only did running increase firing rates in individual neurons, running also changed the structure of activity across populations of cells, resulting in an increase in the entropy of the ensemble activity. Although a maximum entropy model of M/T cell firing patterns recapitulated the small changes in the pairwise interactions between neurons during locomotion, it failed to predict the global structure of population activity when the animal was running. Our results suggest that population activity in the olfactory bulb can be restructured by locomotive behavior, arising from alterations in the functional interactions between neurons.

MATERIALS AND METHODS

Animals

All protocols and procedures were approved by the University Committee on Animal Resources (UCAR) at the University of Rochester and were performed in accordance with the guidelines of the Institutional Animal Care and Use Committee (IACUC) at the University of Rochester. Three female and two male C57Bl6/J mice, age 3–6 mo, were used in this study.

Surgery

Mice were anesthetized with an inhaled 1%–2% isoflurane mixture. The scalp was removed and a three-dimensional (3-D) printed headframe was attached to the dorsal skull surface with veterinary adhesive (Vetbond, The 3M Company, Maplewood, MN) and dental cement (Ortho-Jet Powder and Jet Liquid, Lang Dental Mfg. Co., Wheeling, IL). A metal ground screw was also implanted into the skull. Following surgery, mice were monitored until they recovered from anesthesia. Animals were recovered for 24 h before behavioral habituation. Postoperative analgesia was provided in accordance with approved protocols and animal weight was monitored during the week.

Run Wheel Habituation

For a 5-day period following headframe implantation, mice were placed on a nonmotorized running wheel for 1 h daily. During these sessions, electrophysiological recordings were not performed. The purpose of these sessions was to acclimate the mice to running on a wheel while head fixed. We previously found that following 5 days of exposure, both male and female mice habituate to the run wheel based on their running behavior (36) after which electrophysiology was performed.

Electrophysiology

Mice were anesthetized with 1%–2% inhaled isoflurane and a craniotomy was performed over the right main olfactory bulb using stereotactic coordinates (5 mm rostral, 1 mm lateral, and 1–1.5 mm ventral of bregma). Immediately following the craniotomy, mice were transferred to the running wheel, where they were head-fixed and allowed to recover from anesthesia. A 128-channel nanofabricated silicon electrode array (37) was vertically lowered into the MOB (Fig. 1, *A* and *B*). Extracellular voltage recordings were collected at 30 kHz in the 0.1–3,500 Hz frequency band (Fig. 1*C*). For four of the mice, one recording session was performed. For one mouse, a second recording session in a different region of the MOB was performed. Simultaneously, the running velocity of the mouse was also recorded via a rotational encoder attached to the wheel. All recordings were performed while mice were awake and behaving on the nonmotorized voluntary running wheel. The recording rig was enclosed in a box to minimize interference from ambient odor, light, sound, and electromagnetic noise.

Analysis and Statistics

All data were analyzed using MATLAB using custom code, which is available upon request to the corresponding author. Unless otherwise noted, all summary data report the means and error bars are the standard deviation (SD), and as appropriate, *P* value significance was assessed using Bonferroni correction for multiple pairwise comparisons. Data were collected on five animals across six recording sessions (2 sessions in 1 animal). A total of 676 isolated units were identified across these recordings. The median recording session was 49-min long, providing ~3 million time points of ensemble activity with which to perform statistical analyses for estimating correlations, entropy, and for fitting maximum entropy models

Spike Sorting

Spike sorting was performed as previously described (38). Briefly, putative action potentials, or spikes, were identified as intervals during which the band-passed (500–3,500 Hz) voltage magnitude exceeded 6 standard deviations from baseline. Periods containing voltage artifacts were manually identified and eliminated.

Spikes were assigned to units, or putative single neurons, by concatenating all the spikes on a channel with the signal from eight neighboring channels and projecting them onto a space of principal components (PC) that explained 80% of the variance. Clusters were identified automatically using a mixture of Gaussians (40). We classified single units using a final manual curation which included the following criteria: There should be a total number of spikes > 50 over the recording session. The mean waveform shape should be preserved across the entire recording, fewer than 5% of the interspike intervals should be less than 5 ms, there should be

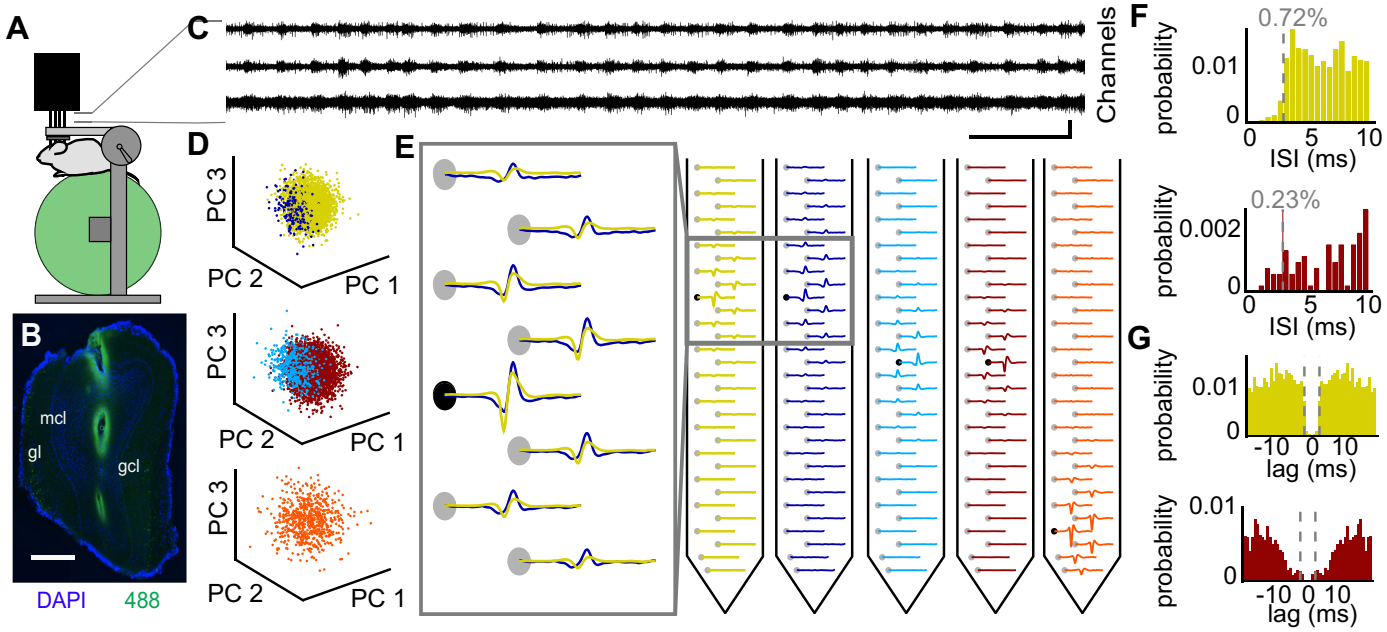

Figure 1. Electrophysiological monitoring of large ensembles of mitral/tufted cells in a head-fixed animal on a run wheel. *A*: schematic of recording population activity from mitral/tufted cells in the main olfactory bulb of awake mice affixed to a run wheel. *B*: coronal section of main olfactory bulb (MOB) showing recording location (labeled by cholera toxin B subunit conjugated to Alexa 488). Scale bar = 100 μm. *C*: bandpass (500–3,500 Hz) voltage trace from 3 channels of 128 channels show spiking activity across multiple contacts. *D*: PCA (principal component analysis) projections of spike waveform clusters used for identifying single units. Each color represents a waveform from *E*, each point is a single spike. *E*: spike waveforms of two units across 8 channels from a single 32 channel shank (*left*) and waveforms across all 32 channels for 5 units show that spiking activity from a single cell can be found across 8-12 contacts (*right*). *F*: interspike interval (ISI) histogram for two units in *D* and *E*. *G*: autocorrelation of spike counts from two units in *D* and *E*. gcl, Granule cell layer; gl, glomerular layer; mcl, mitral cell layer.

fewer than 5% of spikes in the zero-lag spike correlation (+5 ms and −5 ms), and there should be low spike waveform similarity across units as assessed by correlation.

Running Behavior Analysis

The motion of the run wheel was controlled by the mouse, which could ambulate in forward or reverse directions or remain stationary. Wheel movement was converted to a velocity by integrating with a 150-ms time bin in 10-ms steps. Bins in which the velocity exceeded 1 cm/s were classified as running and all other bins were classified as stationary.

Correlations

The pairwise correlation was calculated using the Pearson correlation coefficient. A sliding window was applied to the spike rasters (spike counts were integrated over a 150-ms time bin with a temporal step of 10 ms) to convert the binary spike pattern to a continuous firing rate trace, which was then converted to a *Z*-score. We note that we tried different time windows (10 ms, 50 ms, and 150 ms) and different time steps (1 ms, 5 ms, and 10 ms) and these values did not affect the results of the study. The covariance between the running velocity and the activity of every unit in each animal was calculated using the Pearson correlation coefficient of the continuous firing rate with the *Z*-score of the run velocity (of the 6 recording, 4 had over 100 units and the remaining 2 recordings had 29 and 86 units). Null distributions of correlations were calculated by temporally shuffling spike times and generating instantaneous firing rate time series from the shuffled spike trains. This was done by randomly shuffling the spike rate vector for each unit, which eliminated the temporal relationship with other units and with the animal's behavior but preserved the structure of the autocorrelation.

To assess the correlation between the $\mathbf{h_i}$ term of the maximum entropy model and the firing rate and the $\mathbf{J_{ij}}$, term with the pairwise correlations for each pair of units, we calculated the Pearson correlation coefficient for the two values. As the random resample process resampled the same unit in different draws, the $\mathbf{h_i}$ term on each draw was compared with the firing rate. Similarly the $\mathbf{J_{ij}}$ term for each pair in a resample was compared with the Pearson correlation for that pair of units.

Statistical significance was assessed using Wilcoxon signed-rank test with Bonferroni correction for multiple pairwise comparisons to ensure that differences between running behavior and neuronal firing were not due to chance, as well as to correct for statistical comparisons across multiple animals.

Entropy

The spike train of each unit was binarized using 10 ms nonoverlapping bins. If one or more spikes from a given unit was present in a bin, the bin was assigned a value of 1. If no spikes were present in that bin, it was assigned a value of 0. This resulted in a binary matrix, in which each column describes the state of every neuron in the recorded population at a given time (41–43). The probability distribution of these population states (entropy) was calculated as follows:

$$H = \sum_i -p_i \log_2 p_i \qquad (1)$$

where H is the entropy and p_i is the probability of the ith pattern. For entropy analyses, the overall recorded population

of neurons from each animal was subsampled 500 times. The number of neurons included in the subsample was varied between $n = 3$ neurons and 25 neurons. Entropy for running and stationary epochs was conditioned on the run velocity being greater than 1 cm/s as follows:

$$H_{\text{stationary}} = \sum_{i=1}^{n} -(p_i|\text{stationary})\log_2(p_i|\text{stationary}), \quad (2)$$

$$H_{\text{running}} = \sum_{i=1}^{n} -(p_i|\text{running})\log_2(p_i|\text{running}). \quad (3)$$

Statistical significance was assessed using Wilcoxon signed-rank test with Bonferroni correction for multiple pairwise comparisons. This was done to ensure that differences were significant both within each animal (n = 500 resamples, comparing running vs. stationary for each subsample) and well as across the population (n = 5 animals, 6 recording sessions).

Maximum Entropy Models

The "maxent_toolbox" software (44) was used to fit the maximum entropy models (43, 45). First, the local field terms $\mathbf{h_i}$ and pairwise interaction terms $\mathbf{J_{ij}}$ were computed from the binned spike trains. Greater magnitude of $\mathbf{h_i}$ indicates greater frequency of σ_i independently firing, and greater magnitude of $\mathbf{J_{ij}}$ indicates greater frequency of σ_i and σ_j firing simultaneously The resulting model was then used to predict the probability of each pattern:

$$P_2(\sigma_1, \sigma_2 \ldots, \sigma_n) = \frac{1}{Z} exp\left[\sum_i h_i\sigma_i + \frac{1}{2}\sum_{i\neq j} J_{ij}\sigma_i\sigma_j\right], \quad (4)$$

where σ_i denotes the binary state of each neuron and Z denotes the partition function, which normalizes the pattern probability distribution. The pattern probabilities predicted by the model were then compared with those observed in the data using the Kullback–Liebler divergence (KLD). The data binarization process used for the maximum entropy models is the same as that used for the entropy calculations. For each recording session (n = 6 sessions, n = 5 animals), we randomly drew 100 resamples for each ensemble population (3–19 units). The data were then separated into running and stationary epochs, as was done for the entropy calculations. Statistical significance was assessed using Wilcoxon signed-rank test with Bonferroni correction for multiple pairwise comparisons.

RESULTS

To study the effect of locomotion on spontaneous neuronal population activity, high-density 128-channel arrays were targeted to the MOB in head-fixed C57Bl6/J mice (n = 3 females, 2 males, age 3–6 mo) trained to run on a nonmotorized wheel (Fig. 1, *A* and *B*). Action potentials in the extracellular recordings (Fig. 1*C*) were identified, and single-unit activity was clustered using a mixture-of-Gaussians model (40) (Fig. 1, *D* and *E*). Representative mean waveforms from putative M/T cells across all the channels in the electrode shank (Fig. 1*E*) illustrate the waveform diversity of units, with interspike interval (ISI) distributions (Fig. 1*F*) and autocorrelation functions (Fig. 1*G*) reflecting the quality of spike-sorting (see METHODS). On average, 113 ± 46 well-isolated units were identified per recording session (Fig. 2*A*).

Throughout the recordings, intervals of when the mouse remained stationary were interspersed with epochs of running (interrun interval as defined as the epoch between the end of one run interval and the beginning of another = 6.2 ± 25.6 s, Fig. 2*B*). In all animals, neuronal activity was dynamic both across and within stationary and running epochs (Fig. 2*A*). At the single-animal level, mean firing rates during running were significantly larger than those during stationary epochs in three animals (Bonferroni-corrected $P <$ 0.05, two-sided Wilcoxon signed-rank test, Fig. 2*C*). At the group level, overall firing rates were increased with running ($FR_{stationary}$ = 1.86 ± 1.06 Hz, $FR_{running}$ = 2.10 ± 1.15 Hz, $P <$ 0.05, two-sided Wilcoxon signed-rank test, n = 6, Fig. 2*D*). Although average firing rates across the population increased with running, individual neurons exhibited diverse changes in their activity patterns including both increases and decreases in firing during locomotion. For example, a plot of the run velocity of the animal and the firing rates for three example M/T cells showed units that were negatively correlated, uncorrelated, or positively correlated with running velocity (Fig. 2*E*). The range of correlations observed was significantly different than chance, as determined using temporally shuffled spike trains ($P < 10^{-6}$, two-sample F test, n = 6 recording sessions, Fig. 2*F*).

Whereas the relationship between a neuron's firing rate and the animal's run velocity reflected the impact of behavior on the dynamics of individual M/T cell activity, we next wished to see how this activity was correlated across mitral/tufted cells, a measure sometimes described as the functional coupling. To do this, we calculated the pairwise correlation from the continuous firing rate for every pair of units in each animal during stationary and running epochs (Fig. 3*A*, one example animal). In this example animal, pairwise correlations during running were significantly different than those during stationary epochs (Fig. 3*B*, running = 0.06 ± 0.1, stationary = 0.1 ± 0.1, $P <$ 0.005, n = 143 pairs). Across all animals, we found that the pairwise correlations were significantly different when the animal was running as compared with when they remained stationary (Fig. 3, *B* and *C*, $P <$ 0.0005, n = 5, Bonferroni-corrected Wilcoxon signed-rank test). Consequently, not only did the firing rates of M/T cells change when the animal was running, but the interactions between neurons were also altered.

Statistical descriptions such as firing rate or pairwise correlations can prove informative when describing the activity of single neurons, or pairs of neurons, but in larger populations of cells, it becomes harder to use these metrics to describe overall network activity. Importantly, a number of studies have shown that odor encoding in the bulb is done not by single units, but it relies on the activity of ensembles of mitral and tufted cells from both the same (46) and different glomeruli (47). As our recordings included up to 175 simultaneously recorded units, we wish to use metrics that describe the statistical properties of activity across groups of neurons. Consider for example, a group of N neurons. If we treat an action potential in each cell as a binary event, recorded as a 1 or a 0, then the network of N neurons would have 2^N possible states. For an example recording with 118 units, this would be $2^{118} \approx 10^{40}$ possible states. Recording

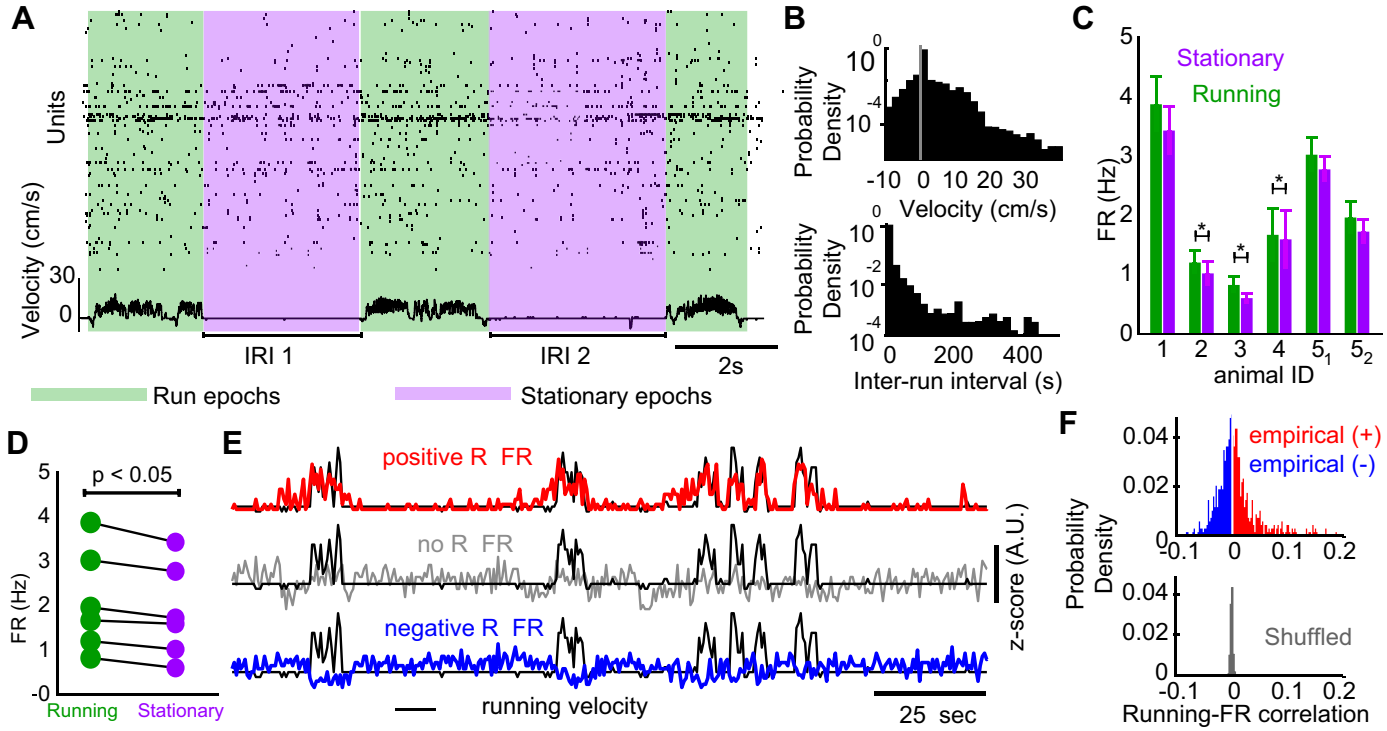

Figure 2. Mitral/tufted (M/T) cell firing was modulated by locomotion. *A*: example trace of ensemble of recorded units while the animal was running (green) vs. when it was stationary (purple). *B*: histogram of run velocity across all animals (*top*) and histogram of interrun intervals (*bottom*). *C*: mean firing rate across units for 6 recording sites across 5 animals. Firing rates were significantly higher in 3 animals when the animal ran. *D*: firing rates were significantly higher on average during running across all recording sites from all animals ($n = 6$). *E*: example traces of unit firing rate, running velocity, and correlation coefficient (*R*) between running and firing rate for a correlated unit (red), uncorrelated unit (gray), and negatively correlated unit (blue). *F*: histogram of correlations between unit firing rate and run velocity (*top*, positive correlated units = red, negatively correlated units = blue; *bottom*, shuffled data = gray). A.U., arbitrary units; FR, firing rate; IRI, interrun interval.

enough data to accurately estimate the probability of each of these states is experimentally intractable. Alternatively, previous studies have shown that subsampling from the full recordings sets to generate populations of neurons between 4 and 20 can provide an appropriate description of the statistical features of network activity (38, 43, 45). Consider a recording of 4 or 10 neurons, which would correspond to a network of 24 = 16 or 210 = 1,024 states, respectively. In these

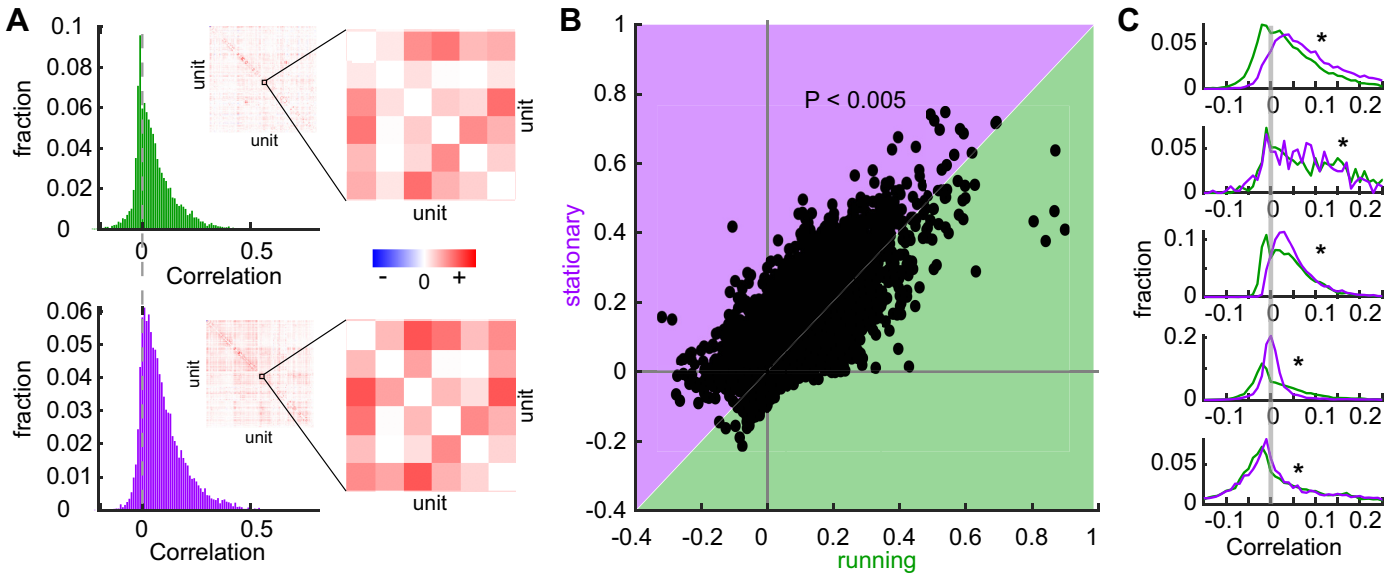

Figure 3. Mitral/tufted (M/T) cell pairwise correlations were significantly different when animal was running. *A*: histogram of M/T cell pairwise correlations for a single animal when the animal was running (*top*) vs. when the animal was stationary (*bottom*). *Inset*: correlation matrix for all pairs (positive correlations, red; negative correlations, blue). *B*: correlated activity during running plotted against correlated activity when the animal was stationary. *C*: histogram of pairwise correlation for running (green) vs. stationary (purple) across five additional recording sessions in a total of five animals show that pairwise interactions were significantly different in all experiments. *$P < 0.05$, two-sided Wilcoxon signed-rank test.

examples, it becomes possible to record neuronal activity for durations that are sufficient to estimate the distribution of states when the animal is running versus when it is stationary. Instead of describing the interactions across all pairs of cells (correlation), such a metric summarizes the consequence of all the interactions across the network. To do this, we first subsampled from each of our recordings (Fig. 4*A*, each circle is a graphic of a single unit) a population of neurons, in this example 4 cells are being resampled from the original population. This was done 500 times, randomly drawing a new subsample from the original data. Within each subsample, we binned the spiking activity in 10-ms windows, where a 1 corresponded to the occurrence of a spike and a 0 corresponded to the absence of a spike, and generated vector pattern, also referred to as a word. Each corresponded to a unique firing pattern across the ensemble. As the number of possible patterns was comparatively small, 16 for instance in a 4-neuron population, we could estimate the probability of seeing any given pattern directly from the data (Fig. 4*B*) during epochs when the animal was running versus when it was stationary. To ensure that our estimates of the pattern probabilities in each animal were not biased due to oversampling some units over others, we confirmed that each cell was equally represented in the random draws (uniform frequency = 1.2% for this recording example, actual sample frequency = 1.16% ± 0.03% in 500 random samples, Fig. 4*C*).

What do these patterns tell us about the structure of population activity in M/T cells that single neuron firing does not? Consider a random subsample of 4 neurons from a single recording, with 24 = 16 possible patterns (Fig. 4*D*). The most commonly occurring word was [0 0 0 0] (no neuron firing), corresponding to pattern 0, regardless of whether the animal was running or not (Fig. 4*D*). By contrast, we did not observe the pattern [1 1 1 1] in this example, corresponding to the simultaneous firing of all neurons regardless of whether the animal was running or stationary (Fig. 4*D*). Interestingly, while we observed the coactivation of triplets of neurons (for example, word [1 1 1 0] or [0 1 1 1] corresponding to patterns 7 and 14, respectively) when the animal was running (Fig. 4*D*, *top*), we found that these patterns did not occur at all when the animal was stationary (Fig. 4*D*, bottom). In this 4-neuron example, we found that there was a significant increase in the occurrence of triplet patterns when the animal was running as compared with when it was stationary ($P < 0.005$, $n = 4$ triplets). Although this example illustrates the differences between triplet activation, a metric statistical dispersion that summarizes all the different patterns, entropy, is more suited to describe the frequencies of word occurrences. The more uniform the occurrence of patterns, the higher the

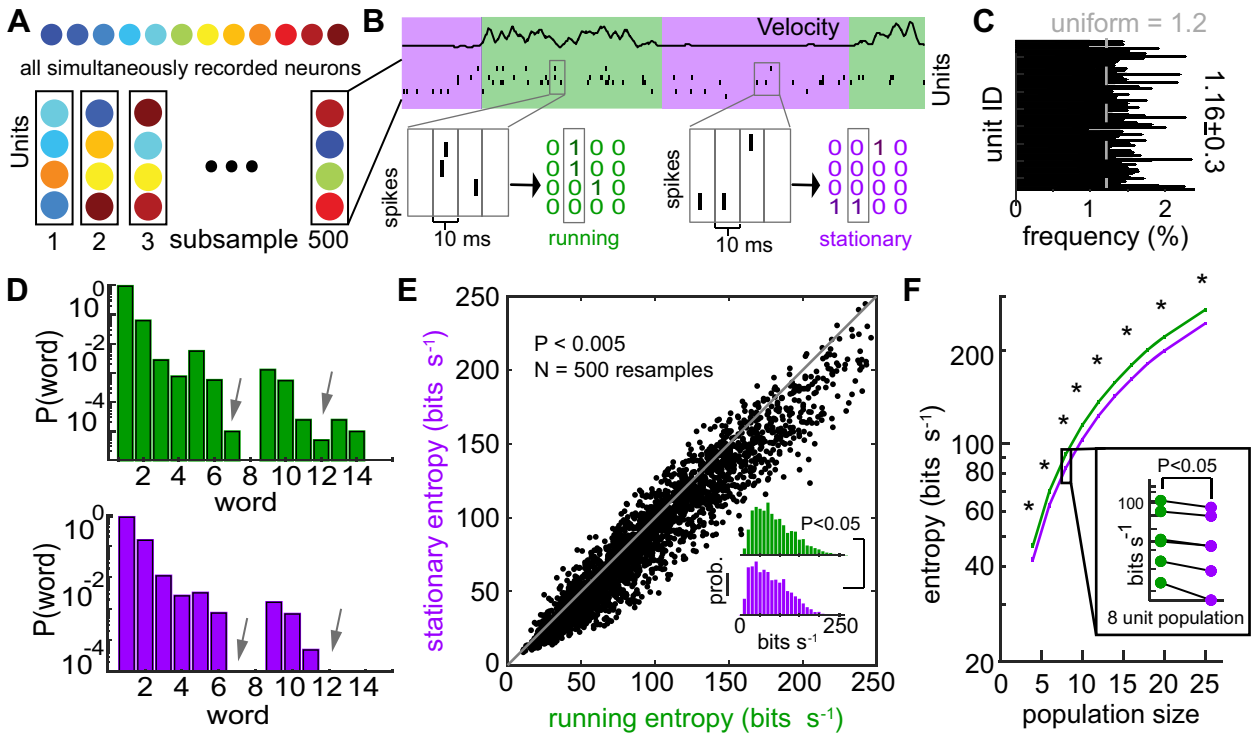

Figure 4. Entropy was greater when animals were running as compared with when they were stationary. *A*: schematic describing random subsamples of neurons to generate example populations to calculate entropy. Each colored dot represents a different neuron and the box corresponds to one example of a random subsample. This process was repeated 500 times. *B*: description of how ensemble activity was converted into binary patterns. Spikes were binned in 10-ms windows and converted to patterns of 1s and 0s conditioned on periods when the animals were running vs. when they were stationary. *C*: histogram of the frequency with which each neuron was randomly sampled reveals that entropy calculations were not biased by the subsampling process. The mean frequency of random sampling was not different than a uniform distribution. *D*: probability of seeing 1 of 16 patterns when the animal was running vs. when it was stationary. *E*: entropy for 500 subsamples of an 8-neuron population in a single animal during running vs. stationary epochs. *Inset*: histogram of entropy for running vs. stationary epochs. *F*: entropy for different subpopulations sizes from 4 to 25 units (500 samples/animal/subpopulation size) shows that entropy was significantly higher when the animal was running as compared with when it was stationary. *Inset*: mean entropy was lower when stationary as compared with running at the single animal level. *$P < 0.005$, two-sided Wilcoxon signed-rank test.

entropy. The higher the entropy, the greater the diversity of patterns that occurs across the population. For 500 resamples of an 8-unit subpopulation in a single animal, entropy (denoted H) was greater when the animal was running as compared with when the animal was stationary ($H_{stationary}$ = 77.4 ± 28 bits/s, $H_{running}$ =85.7 ± 35 bits/s, $P < 0.05$, two-sided Wilcoxon signed-rank test, Fig. 4*E*). The increase in entropy was also significant across all recording sessions on a per animal basis ($H_{stationary}$ = 82.7 + 11 bits/s, $H_{running}$ = 91.8 ± 13 bits/s, $P < 0.005$, two-sided Wilcoxon signed-rank test, n = 5 animals, 6 recording sites, Fig. 4*F*). Furthermore, the entropy was significantly larger when the animal was running over a range of different numbers of neurons in the subpopulation (n = 500 resamples animal, n = 5 animals, n = 6 total recording sites, $P < 0.005$ for populations from 4–25 neurons, two-sided Wilcoxon signed-rank test with Bonferroni correction, Fig. 4*G*). In addition, the entropy was larger during locomotion across a variety of bin sizes (50 ms, 100 ms, data not shown), meaning the number of patterns of spontaneous activity when the animal was locomoting were larger. Locomotion resulted in a restructuring of population activity across M/T cells, with larger groups of coactivated neurons resulting in a higher entropy in the population when the animal was running as compared with when it was stationary.

How then do we relate these findings about population activity and network state to the firing rates of individual neurons or the pairwise interactions of cells, statistical measures that have historically been used to summarize the activity of mitral and tufted cells in the bulb? For instance, how likely are we to estimate the overall structure of the activity patterns (the probability of seeing different patterns), given what we know about the firing rate and/or the pairwise interactions of M/T cells? Or, put another way, can a model built from simple metrics of neuronal activity predict the frequency of different patterns of activity occurring across the whole population. The maximum entropy method is one such approach to tackle the question. In this framework, spiking data are binarized into patterns of 1s and 0s, and from these patterns, statistical features are extracted (Fig. 5*A*). A maximum entropy model is used to generate predictions of the patterns that occur (synthetic data) based on the constraints of those statistical features. These synthetic data are then compared with the experimental recordings to assess the explanatory power of model, and by proxy, the features that go into the model (Fig. 5*A*).

Consider the simplest model of population activity, one where each neuron is independently firing. In this first-order model, the probability of seeing any given pattern in the

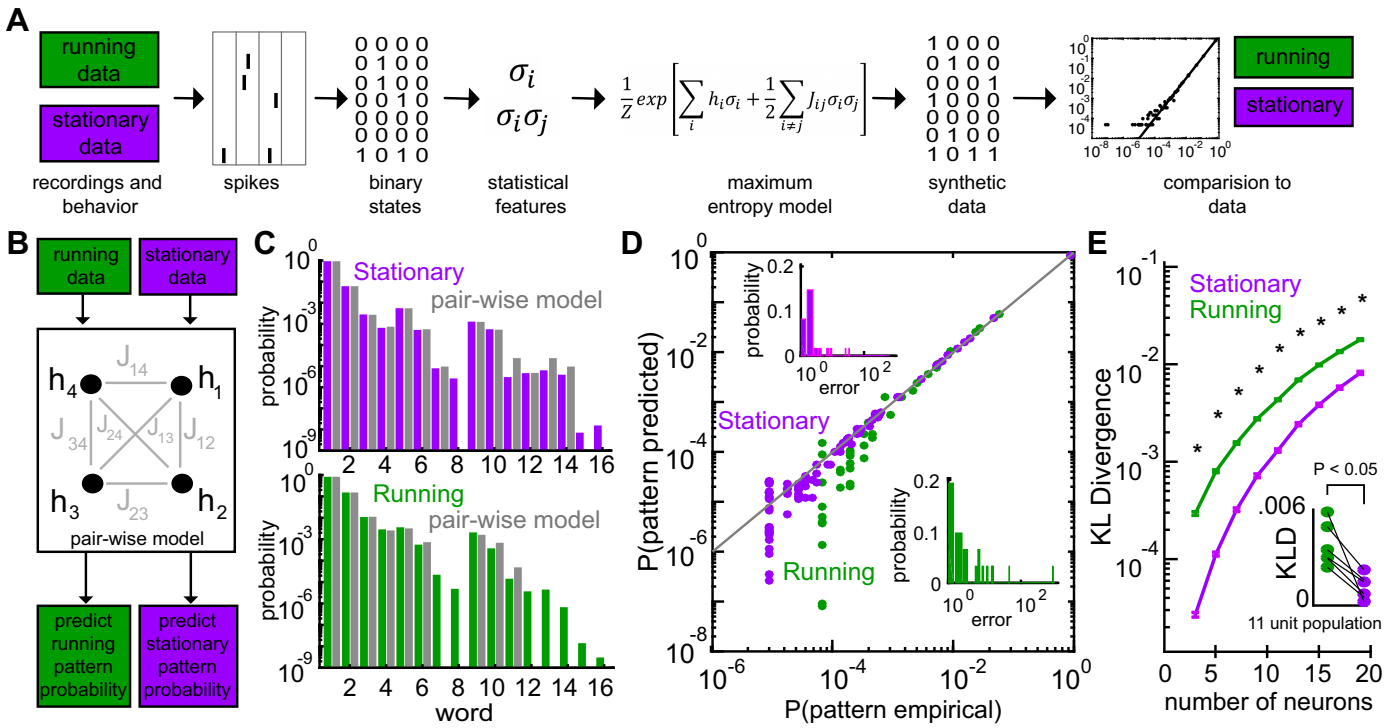

Figure 5. Pairwise maximum entropy models were better at fitting mitral/tufted (M/T) cell ensemble activity when the animal was stationary as compared with when it was running. *A*: schematic of the process for converting raw spiking data into binary states, and then estimating statistical features of neuronal activity that are used by a maximum entropy model to predict the distribution of network states. *B*: schematic of features in a pairwise maximum entropy model of a 4-neuron population. *C*: example histogram of patterns of activity observed in a 4-neuron population (24 = 16 possible patterns) when the animal was stationary (*bottom*) versus when it was running (*top*). Purple and green bar graphs correspond to the actual probabilities observed from the recordings and gray bar graphs correspond to the probabilities estimated from the maximum entropy model. *D*: for an example 8-unit population, the rate occurrence of each firing pattern from the pairwise maximum entropy model was plotted against the observed data for running (green) and stationary (purple) epochs. *Insets*: histograms of prediction error of rate of occurrence of the firing patterns showed that error was higher when the animal was running. *E*: Kullback–Leibler divergence (KLD), which measures the goodness of pairwise maximum entropy model prediction for different subpopulations sizes from 3 to 19 units during running vs. stationary epochs. *$P < 0.05$, two-sided Wilcoxon signed-rank test with Bonferroni correction. *Inset*: mean KLD for each recording session during running vs. stationary epochs for a 11-neuron subpopulation.

J Neurophysiol • doi:10.1152/jn.00464.2020 • www.jn.org

network would be completely described by the on and off probabilities of each cell (their firing rate). Consistent with reports across a number of other neural circuits including the retina of the salamander (43), the primary visual cortex of the nonhuman primate (45) and the hippocampus of the mouse (48), a first-order maximum entropy model of M/T cell activity was poor at estimating the probability of patterns that occurred regardless of whether the animal was running or stationary (data not shown). This is not surprising given that M/T cells are connected to one another in a number of ways, including but not limited to inhibitory granule cells (49–51) via dendrodendritic synapses (25, 52–54), all of which impose correlations on the activity of neurons (46, 52, 54, 55). Ideally then, a model that aims to predict the global structure of activity should include not only the firing rates, but also the functional interactions between neurons in the bulb. We therefore used a second-order maximum entropy model, one that uses only two features to make predictions about the global structure of M/T activity. The first feature was represented as the local field term ($\mathbf{h_i}$), which was analogous to the mean firing rate of the cell likely shaped by a number of individual neuron properties such as the intrinsic excitability, the biophysics, etc. (56–58). As the local field term $\mathbf{h_i}$, was a measure of how likely the cell was to spike, the more negative the value, the less active the neuron. The second feature of the pairwise model, the coupling term ($\mathbf{J_{ij}}$) captured the strength of correlations between pairs of neurons, reflecting all of the cell and network properties that influenced correlations (46, 50, 51, 59, 60) (Fig. 5*B*).

The second-order maximum entropy model allowed us to determine how good these two features of activity were in predicting the occurrences of the global structure of M/T cells. A good model would tell us that these two features are sufficient to explain the overall structure of dynamics in the bulb as it would predict occurrences of different patterns that matched those observed in the data. Again, consider an example 4-neuron population subsampled from a recording of 143 simultaneous cells. The probability of seeing each of the 16 possible patterns while the animal was stationary (Fig. 5*C*, *top*, purple bars) and when it was running (Fig. 5*C*, *bottom*, green bars) described how frequently we saw each pattern of activity in this example. When we compared these probabilities to what was predicted by the maximum entropy models (Fig. 5*C*, gray bars), a number of trends became apparent. First, for both running and stationary epochs, the two features of the second-order model (firing rate and correlation) were sufficient to predict the frequency of seeing some patterns (*patterns 1–4*, Fig. 5*C*). However, the maximum entropy model using features of activity extracted when the animal was running was poor at predicting the frequency with which other patterns occurred (*patterns 12–14*, Fig. 5*C*). By contrast, a maximum entropy model using features extracted when the animal was stationary was much better at predicting the frequency which the same patterns occurred (Fig. 5*C*, *top*, gray bars). To visualize the goodness of prediction between the model and the data, we plotted the frequency of seeing each pattern in an 8-neuron population (256 patterns) for running and stationary epochs (Fig. 5*D*). Each point corresponds to a different pattern, and the closer to the unity line (black) the point, the better the model was at predicting the frequency with which that pattern occurred in the data. In this example, predictions of patterns from the model during running were worse than those during stationary epochs (Fig. 5*D*). These errors in prediction during running epochs may seem small at first glance, a model, for example, predicts that some patterns occur at a probability of 10^{-6}. However, the pattern was actually observed to occur with a probability of 10^{-4}, meaning that the error was on the order of 100-fold (Fig. 5*D*, *inset*). One way to quantify the error in model's prediction was by calculating the Kullback–Leibler divergence (KLD), a measure of the "distance" between the predicted occurrences of patterns made by the model and the actual observations about the frequency of those patterns occurring. The smaller the KLD, the better the model was at estimating the global structure of the network from simple features. For an 11-unit population, the KLD was larger for running epochs as compared with stationary epochs, indicating that the fit was worse when the animals ran ($KLD_{stationary} = 0.0012 \pm 0.0008$, $KLD_{running} = 0.0040 \pm 0.0015$, $P < 0.05$, two-sided Wilcoxon signed-rank test, $n = 6$, Fig. 5*E*, *inset*). Across a range of subpopulation sizes (3–19 units), the pairwise maximum entropy model was worse at predicting the global patterns of activity when the animal was running as compared with when it was stationary at both the group level and in individual animals ($P < 0.05$, two-sided Wilcoxon signed-rank test with Bonferroni correction, $n = 100$ resamples/recording/population size, $n = 5$ animals, 6 recording sessions, Fig. 5*E*). Our results revealed that while the features of firing rate and pairwise correlations were sufficient to explain the statistics of population activity when the animal was stationary, these same features failed to explain the global structure of activity when the animals were running. Thus a shift in the organization of spontaneous activity in the bulb occurred based on whether the animal was stationary or running.

To ensure that the features extracted by the maximum entropy model fit with what we observed in both the firing rates and the pairwise correlation data, we examined the mathematical structure that went into the model, the $\mathbf{h_i}$ and $\mathbf{J_{ij}}$ terms. First, as the local field term, $\mathbf{h_i}$, approximated the mean activity of the neuron, we confirmed that this was the case by comparing the values from model to the spike rate (Fig. 6*A*, running $R = 0.95$, stationary $R = 0.96$, $n = 6$ recordings from 5 animals, 100 resamples per animal). Furthermore, we found that the local field term $\mathbf{h_i}$, was significantly higher during running as compared with when the animal was stationary ($\mathbf{h_{i,running}} = -5.20 \pm 1.67$, $\mathbf{h_{i,stationary}} = -5.42 \pm 1.81$, $P < 0.005$, two-sided Wilcoxon signed-rank test, Fig. 6*B*) across subpopulations ranging in size from 3 to 19 neurons ($P < 10^{-6}$, two-sided Wilcoxon signed-rank test with Bonferroni correction, Fig. 6*C*), consistent with the model accurately capturing differences in mean firing rates during running and remained period.

Similarly, we found that the local field term $\mathbf{J_{ij}}$, which reflects the interactions between pairs of neurons in the model, corresponded to the correlations in spiking activity across pairs (Fig. 6*D*, running $R = 0.74$, stationary $R = 0.64$). Furthermore, the distributions of the $\mathbf{J_{ij}}$ terms were significantly decreased during running as compared with when the animal was stationary, again reflective of the significant differences in correlations we observed ($\mathbf{J_{ij,stationary}} = 0.41 \pm 1.15$; $\mathbf{J_{ij}}_{running} = -0.08 \pm 0.95$, $P < 0.005$, two-sided Wilcoxon signed-rank test, Fig. 6*E*). The differences in the $\mathbf{J_{ij}}$ term

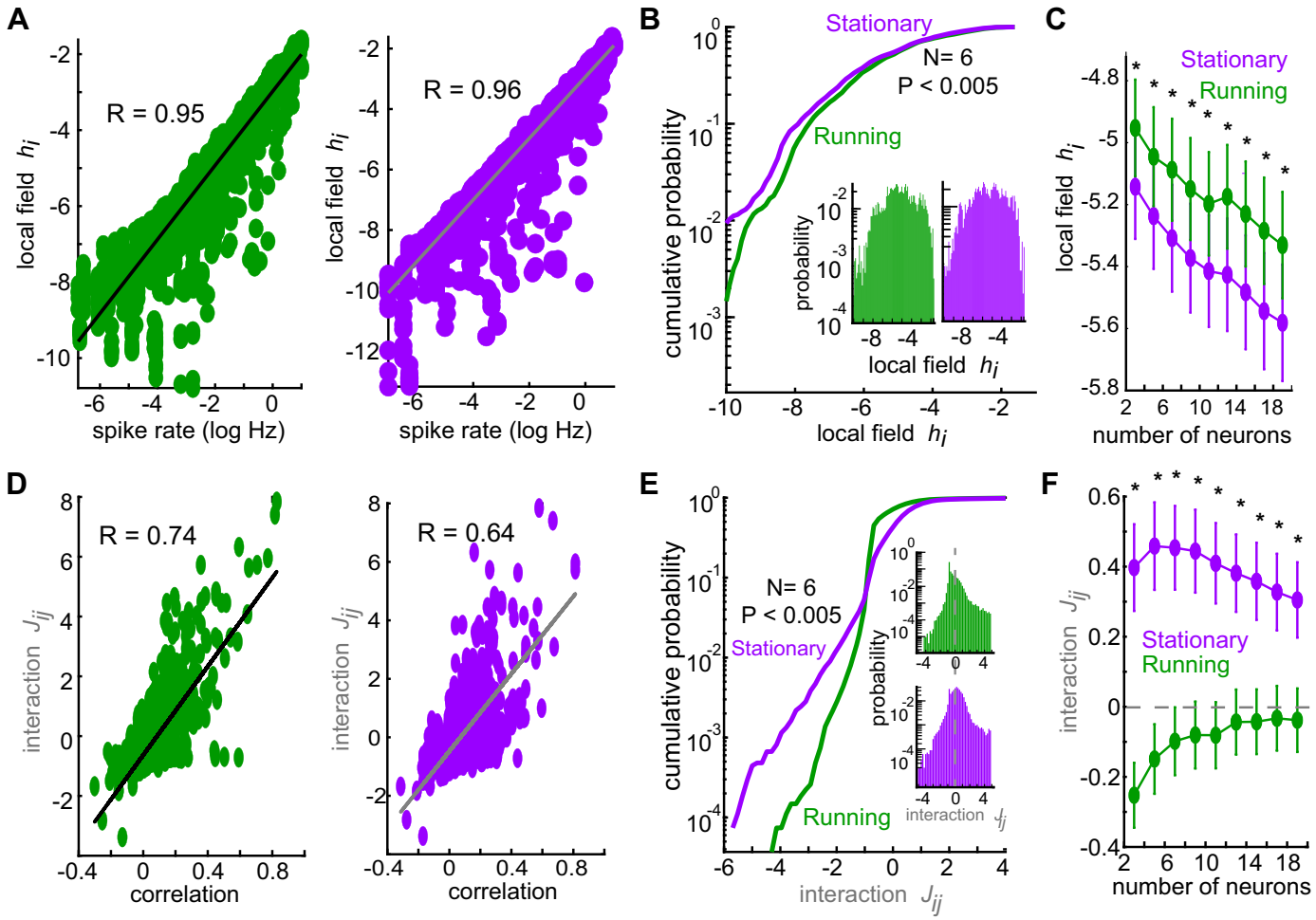

Figure 6. Maximum entropy models successfully identify different features of network activity when the animal is running vs. when it is stationary. *A*: correspondence of the local field term in the maximum entropy model to the spike rate during running epochs (*left*, green) and stationary epochs (*right*, purple) for all experiments. *B*: cumulative histogram of local field term of pairwise maximum entropy model from a single animal across multiple resamples of an 8-unit subpopulation. *Inset*: histogram of local field term of pairwise maximum entropy model from all recording sessions. *C*: mean local field term for different subpopulation sizes. $*P < 10^{-6}$, two-sided Wilcoxon signed-rank test with Bonferroni correction. *D*: correspondence of the interaction term in the maximum entropy model to the pairwise correlation in spike count during running epochs (*left*, green) and stationary epochs (*right*, purple) for all experiments. *E*: cumulative histogram of interaction terms of pairwise maximum entropy model from a single animal across multiple resamples of an 8-unit subpopulation. *Inset*: histogram of local field term of pairwise maximum entropy model from all recording sessions. *F*: mean interaction term for different subpopulation sizes. $*P < 10^{-6}$, two-sided Wilcoxon signed-rank test with Bonferroni correction.

were significant across an array of subpopulation sizes ($P <$ 0.005 for 3–19 neurons, two-sided Wilcoxon signed-rank test with Bonferroni correction, Fig. 6*F*). These data taken together with previous results revealed two important features of the statistics of spontaneous activity. First, pairwise interactions were poorer at predicting network state when the animal was running as compared with when it was stationary. Second, although the maximum entropy model accurately learned important features of this activity, such as the firing rate of individual cells or the pairwise interactions, these features were significantly worse at predicting the global statistical structure of coactivated neurons when the animals were running, with errors often of many log orders.

DISCUSSION

In this study, we found that mitral/tufted cell population activity in the main olfactory bulb of the mouse changed during the animal's locomotion. In addition to increases in firing rates of individual neurons, the entropy of population activity was increased when the animal ran, resulting in an increase in the dimensionality of the ensemble activity. A second-order maximum entropy model fit to the population activity revealed that pairwise interactions could explain the global structure of the firing when the animal was stationary, but the explanatory power of these pairwise interactions diminished when the animal ran. We therefore suggest that running triggers higher order (3rd, 4th, etc.) interactions between M/T cells, reshaping the global structure of activity within the bulb.

What do these changes in neuronal population activity signify in terms of olfactory function? Without recording responses to arrays of odors while the animal is running versus when it remains stationary, the information content of the neuronal ensemble cannot be extrapolated from the entropy. These information estimates depend heavily on how

the stimulus domain is partitioned (how different are the odors, odor classes, concentrations, etc.) as well as the sampling (number of stimuli presented, number of trials, etc.) (61–65), questions we leave for future work. Furthermore, although we were not able to measure sniffing, a feature of neuronal responses in the bulb (66), recent studies demonstrate the sniffing in head fixed animals may be different than freely behaving animals (67). Although sniffing and or whisking could give rise to changes in the activity of individual M/T cells (18–20, 66), we focused on assessing "how" any behavioral changes during running could influence neural population activity, and what this might mean for general principles of encoding.

Studies in visual cortex (5, 68), auditory cortex (7, 69), and the olfactory bulb (70, 71) suggest that patterns of spontaneous activity recapitulate patterns of activity in response to sensory stimuli (6, 68, 72), effectively outlining the realm of possible patterns that "can" occur (7, 71). As entropy increases and pairwise correlations decrease during locomotion, our results suggest that the realm of possible patterns of activity when the animal was running is larger. If the combinations of spontaneous activity patterns in the bulb define a manifold within the overall space of possible patterns, the manifold may be differentially altered or expanded during running. A number of studies suggest that odor-evoked activity either extends from or alters the structure of the manifold (55, 59, 71, 73).

Our work also points to important mechanisms about how locomotor behavior sculpts neural activity in the bulb. We extracted features of neuronal activity such as the statistics of individual neuron firing rate and the structure of pairwise interactions between M/T cells in the bulb. These features were then used to predict the probability of seeing specific patterns of activity across large ensembles of neurons using a second-order maximum entropy model. Although the structure of activity when the animal was stationary could be predicted by the model, the model failed to recapitulate the observed activity patterns when the animal was running. Maximum entropy models can be thought of as a way to generate null hypotheses about the functional connectivity within neural circuits (74). In the retina, for instance, pairwise maximum entropy models that use individual features, such as the firing rate of neurons and the correlations between cells, are sufficient to account for the joint activity of ensembles of neurons (43, 75). By contrast, these same pairwise interaction models fail to account for the joint activity of populations as small as 5 neurons in the primary visual cortex (45) pointing to higher order structure (3rd, 4th order) in population activity, possibly sculpted by local inhibitory interneurons. These differences in the structure of neuronal activity are not surprising given the differences in the organization of the circuits in the salamander retina as opposed to the primate visual cortex. Interestingly, our work suggests that differences in the structure of population activity may also be dynamically gated by behavior within a single area. In the bulb, M/T cells are interconnected with a large network of inhibitory granule cells (49, 51, 76–78), which receive centrifugal inputs from a number of regions including the anterior olfactory nucleus (AON), the piriform cortex, the horizontal diagonal band, and the raphe nucleus (27, 29, 79, 80). In addition to these feedback projections, monosynaptic inputs from both the ventral CA1 (vCA1) region of the hippocampus and the entorhinal cortex (30, 31) would be candidate circuits that relay locomotion information to the bulb. Locomotion may therefore influence the state of network, altering the degree to which pairwise interactions or higher order interactions structure M/T cell firing via inhibitory granule cells. Importantly, we have uncovered that the structure of activity in the bulb was highly flexible, explained in some cases (when the animal is stationary) by pairwise interactions, but not so in other cases (when the animal is running). Thus, locomotor behavior may influence the "initial state" of the network, determining how odor-evoked activity patterns evolve. What might be the downstream consequences of such a restructuring of the activity in the bulb during locomotion? Recent evidence suggests that spontaneous activity in the olfactory cortex (piriform cortex) is driven by the firing of neurons in the bulb (81). Changes in the structure of spontaneous activity in the bulb during locomotion would dynamically gate the range of olfactory coding in the piriform cortex.

We caution that how locomotion is defined in this work is experimentally constrained, as animals are head-fixed and run on a cylinder, with behavior delineated into epochs of stationary versus running. Nonetheless, these experimental distinctions between "stationary" and "running" may correspond to ethologically different behavioral modes. Locomotion, for instance, is necessary in odor navigation and tracking (34, 35), while animals are often stationary when sniffing a single object in service of odor discrimination or odor identification (82–84). These different behavioral modes may be supported by different underlying coding strategies or may include information about behavior itself in the code relayed by M/T cells. By altering the extent to which either firing rate or correlation defines the structure of spontaneous activity, our results suggest that circuits in the bulb are highly flexible to support different modes of coding, operating within a dynamic high-dimensional space shaped by the animal's behavior (9).

GRANTS

K.P. was supported by National Science Foundation (NSF) CAREER (1749772), National Institute of Mental Health (NIMH) (Grant R01MH11392), the Schmitt Foundation, and the Cystinosis Research Foundation. R.C.G. was supported by National Institute of Neurological Disorders and Stroke (NINDS) (Grant U19NS112953) and National Institute on Deafness and Other Communication Disorders (NIDCD) (Grant R01DC018455). U.C. was funded by National Institute of General Medical Sciences (NIGMS) (Grant T32 GM007356).

DISCLOSURES

No conflicts of interest, financial or otherwise, are declared by the authors.

AUTHORS CONTRIBUTIONS

K.P. conceived and designed research; E.J.W.C. and K.P. performed experiments; U.C., S.W., E.L., R.C.G., and K.P. analyzed data; U.C. and K.P. interpreted results of experiments; U.C. and K.P. prepared figures; U.C. and K.P. drafted manuscript; U.C., E.J.W.C., S.W., E.L., R.C.G., and K.P. edited and revised manuscript;

U.C., E.J.W.C., S.W., E.L., R.C.G., and K.P. approved final version of manuscript.

REFERENCES

1. **Constantinople CM**, **Bruno RM.** Effects and mechanisms of wakefulness on local cortical networks. *Neuron* 69: 1061–1068, 2011. doi:10.1016/j.neuron.2011.02.040.
2. **Dadarlat MC**, **Stryker MP.** Locomotion enhances neural encoding of visual stimuli in mouse V1. *J Neurosci* 37: 3764–3775, 2017. doi:10.1523/JNEUROSCI.2728-16.2017.
3. **Dipoppa M**, **Ranson A**, **Krumin M**, **Pachitariu M**, **Carandini M**, **Harris KD.** Vision and locomotion shape the interactions between neuron types in mouse visual cortex. *Neuron* 98: 602–615.e8, 2018. doi:10.1016/j.neuron.2018.03.037.
4. **Vinck M**, **Batista-Brito R**, **Knoblich U**, **Cardin JA.** Arousal and locomotion make distinct contributions to cortical activity patterns and visual encoding. *Neuron* 86: 740–754, 2015. doi:10.1016/j.neuron.2015.03.028.
5. **Niell CM**, **Stryker MP.** Modulation of visual responses by behavioral state in mouse visual cortex. *Neuron* 65: 472–479, 2010. doi:10.1016/j.neuron.2010.01.033.
6. **Tsodyks M**, **Kenet T**, **Grinvald A**, **Arieli A.** Linking spontaneous activity of single cortical neurons and the underlying functional architecture. *Science* 286: 1943–1946, 1999. doi:10.1126/science.286.5446.1943.
7. **Luczak A**, **Barthó P**, **Harris KD.** Spontaneous events outline the realm of possible sensory responses in neocortical populations. *Neuron* 62: 413–425, 2009. doi:10.1016/j.neuron.2009.03.014.
8. **Stringer C**, **Pachitariu M**, **Steinmetz N**, **Reddy CB**, **Carandini M**, **Harris KD.** Spontaneous behaviors drive multidimensional, brainwide activity. *Science* 364: 255, 2019. doi:10.1126/science.aav7893.
9. **Tsuno Y**, **Mori K.** Behavioral state-dependent changes in the information processing mode in the olfactory system. *Commun Integr Biol* 2: 362–364, 2009. doi:10.4161/cib.2.4.8719.
10. **Wilson RI**, **Mainen ZF.** Early events in olfactory processing. *Annu Rev Neurosci* 29: 163–201, 2006. doi:10.1146/annurev.neuro.29.051605.112950.
11. **Rinberg D**, **Koulakov A**, **Gelperin A.** Sparse odor coding in awake behaving mice. *J Neurosci* 26: 8857–8865, 2006. doi:10.1523/JNEUROSCI.0884-06.2006.
12. **Abraham NM**, **Egger V**, **Shimshek DR**, **Renden R**, **Fukunaga I**, **Sprengel R**, **Seeburg PH**, **Klugmann M**, **Margrie TW**, **Schaefer AT**, **Kuner T.** Synaptic inhibition in the olfactory bulb accelerates odor discrimination in mice. *Neuron* 65: 399–411, 2010. doi:10.1016/j.neuron.2010.01.009.
13. **Kobayakawa K**, **Kobayakawa R**, **Matsumoto H**, **Oka Y**, **Imai T**, **Ikawa M**, **Okabe M**, **Ikeda T**, **Itohara S**, **Kikusui T**, **Mori K**, **Sakano H.** Innate versus learned odour processing in the mouse olfactory bulb. *Nature* 450: 503–508, 2007. doi:10.1038/nature06281.
14. **Smear M**, **Resulaj A**, **Zhang J**, **Bozza T**, **Rinberg D.** Multiple perceptible signals from a single olfactory glomerulus. *Nat Neurosci* 16: 1687–1691, 2013. doi:10.1038/nn.3519.
15. **Doucette W**, **Gire DH**, **Whitesell J**, **Carmean V**, **Lucero MT**, **Restrepo D.** Associative cortex features in the first olfactory brain relay station. *Neuron* 69: 1176–1187, 2011. doi:10.1016/j.neuron.2011.02.024.
16. **Doucette W**, **Restrepo D.** Profound context-dependent plasticity of mitral cell responses in olfactory bulb. *PLoS Biol* 6: e258, 2008. doi:10.1371/journal.pbio.0060258.
17. **Kay LM**, **Laurent G.** Odor- and context-dependent modulation of mitral cell activity in behaving rats. *Nat Neurosci* 2: 1003–1009, 1999. doi:10.1038/14801.
18. **Carey RM**, **Wachowiak M.** Effect of sniffing on the temporal structure of mitral/tufted cell output from the olfactory bulb. *J Neurosci* 31: 10615–10626, 2011. doi:10.1523/JNEUROSCI.1805-11.2011.
19. **Kleinfeld D**, **Deschênes M**, **Wang F**, **Moore JD.** More than a rhythm of life: breathing as a binder of orofacial sensation. *Nat Neurosci* 17: 647–651, 2014. doi:10.1038/nn.3693.
20. **Moore JD**, **Deschênes M**, **Furuta T**, **Huber D**, **Smear MC**, **Demers M**, **Kleinfeld D.** Hierarchy of orofacial rhythms revealed through whisking and breathing. *Nature* 497: 205–210, 2013. doi:10.1038/nature12076.
21. **Sofroniew NJ**, **Cohen JD**, **Lee AK**, **Svoboda K.** Natural whisker-guided behavior by head-fixed mice in tactile virtual reality. *J Neurosci* 34: 9537–9550, 2014. doi:10.1523/JNEUROSCI.0712-14.2014.
22. **Sofroniew NJ**, **Svoboda K.** Whisking. *Curr Biol* 25: R137–R140, 2015. doi:10.1016/j.cub.2015.01.008.
23. **Verhagen JV**, **Wesson DW**, **Netoff TI**, **White JA**, **Wachowiak M.** Sniffing controls an adaptive filter of sensory input to the olfactory bulb. *Nat Neurosci* 10: 631–639, 2007. doi:10.1038/nn1892.
24. **Murthy VN.** Olfactory maps in the brain. *Annu Rev Neurosci* 34: 233–258, 2011. doi:10.1146/annurev-neuro-061010-113738.
25. **Tsuno Y**, **Kashiwadani H**, **Mori K.** Behavioral state regulation of dendrodendritic synaptic inhibition in the olfactory bulb. *J Neurosci* 28: 9227–9238, 2008. doi:10.1523/JNEUROSCI.1576-08.2008.
26. **Padmanabhan K**, **Osakada F**, **Tarabrina A**, **Kizer E**, **Callaway EM**, **Gage FH**, **Sejnowski TJ.** Diverse representations of olfactory information in centrifugal feedback projections. *J Neurosci* 36: 7535–7545, 2016. doi:10.1523/JNEUROSCI.3358-15.2016.
27. **Price JL**, **Powell TP.** An experimental study of the origin and the course of the centrifugal fibres to the olfactory bulb in the rat. *J Anat* 107: 215–237, 1970.
28. **Price JL**, **Powell TP.** Certain observations on the olfactory pathway. *J Anat* 110: 105–126, 1971.
29. **Shipley MT**, **Adamek GD.** The connections of the mouse olfactory bulb: a study using orthograde and retrograde transport of wheat germ agglutinin conjugated to horseradish peroxidase. *Brain Res Bull* 12: 669–688, 1984. doi:10.1016/0361-9230(84)90148-5.
30. **Davis BJ**, **Macrides F.** The organization of centrifugal projections from the anterior olfactory nucleus, ventral hippocampal rudiment, and piriform cortex to the main olfactory bulb in the hamster: an autoradiographic study. *J Comp Neurol* 203: 475–493, 1981. doi:10.1002/cne.902030310.
31. **Padmanabhan K**, **Osakada F**, **Tarabrina A**, **Kizer E**, **Callaway EM**, **Gage FH**, **Sejnowski TJ.** Centrifugal inputs to the main olfactory bulb revealed through whole brain circuit-mapping. *Front Neuroanat* 12: 115, 2019. doi:10.3389/fnana.2018.00115.
32. **Gourevitch B**, **Kay LM**, **Martin C.** Directional coupling from the olfactory bulb to the hippocampus during a go/no-go odor discrimination task. *J Neurophysiol* 103: 2633–2641, 2010. doi:10.1152/jn.01075.2009.
33. **Erisken S**, **Vaiceliunaite A**, **Jurjut O**, **Fiorini M**, **Katzner S**, **Busse L.** Effects of locomotion extend throughout the mouse early visual system. *Curr Biol* 24: 2899–2907, 2014. doi:10.1016/j.cub.2014.10.045.
34. **Gire DH**, **Kapoor V**, **Arrighi-Allisan A**, **Seminara A**, **Murthy VN.** Mice develop efficient strategies for foraging and navigation using complex natural stimuli. *Curr Biol* 26: 1261–1273, 2016. doi:10.1016/j.cub.2016.03.040.
35. **Khan AG**, **Sarangi M**, **Bhalla US.** Rats track odour trails accurately using a multi-layered strategy with near-optimal sampling. *Nat Commun* 3: 703, 2012. doi:10.1038/ncomms1712.
36. **Warner EJ**, **Padmanabhan K.** Sex differences in head-fixed voluntary running behavior in C57BL/6J mice. *Eur J Neurosci* 51: 721–730, 2020. doi:10.1111/ejn.14654.
37. **Du J**, **Blanche TJ**, **Harrison RR**, **Lester HA**, **Masmanidis SC.** Multiplexed, high density electrophysiology with nanofabricated neural probes. *PLoS One* 6: e26204, 2011. doi:10.1371/journal.pone.0026204.
38. **Chockanathan U**, **Warner EJ**, **Turpin L**, **O'Banion MK**, **Padmanabhan K.** Altered dorsal CA1 neuronal population coding in the APP/PS1 mouse model of Alzheimer's disease. *Sci Rep* 10: 1077, 2020. doi:10.1038/s41598-020-58038-y.
40. **Lewicki MS.** A review of methods for spike sorting: the detection and classification of neural action potentials. *Network* 9: R53–R78, 1998.
41. **Pryluk R**, **Kfir Y**, **Pryluk R**, **Kfir Y**, **Gelbard-Sagiv H**, **Fried I**, **Paz R.** A tradeoff in the neural code across regions and species. *Cell* 176: 597–609.e18, 2019. doi:10.1016/j.cell.2018.12.032.
42. **de Ruyter van Steveninck RR**, **Lewen GD**, **Strong SP**, **Koberle R**, **Bialek W.** Reproducibility and variability in neural spike trains. *Science* 275: 1805–1808, 1997. doi:10.1126/science.275.5307.1805.
43. **Schneidman E**, **Berry MJ 2nd**, **Segev R**, **Bialek W.** Weak pairwise correlations imply strongly correlated network states in a neural population. *Nature* 440: 1007–1012, 2006. doi:10.1038/nature04701.

44. **Maoz O**, **Schneidman E.** maxent_toolbox: Maximum entropy toolbox for MATLAB, version 1.0.2. 2017. http://doi.org/10.5281/zenodo.191625.
45. **Ohiorhenuan IE**, **Mechler F**, **Purpura KP**, **Schmid AM**, **Hu Q**, **Victor JD.** Sparse coding and high-order correlations in fine-scale cortical networks. *Nature* 466: 617–621, 2010. doi:10.1038/nature09178.
46. **Dhawale AK**, **Hagiwara A**, **Bhalla US**, **Murthy VN**, **Albeanu DF.** Non-redundant odor coding by sister mitral cells revealed by light addressable glomeruli in the mouse. *Nat Neurosci* 13: 1404–1412, 2010. doi:10.1038/nn.2673.
47. **Gerkin RC**, **Tripathy SJ**, **Urban NN.** Origins of correlated spiking in the mammalian olfactory bulb. *Proc Natl Acad Sci USA* 110: 17083–17088, 2013. doi:10.1073/pnas.1303830110.
48. **Meshulam L**, **Gauthier JL**, **Brody CD**, **Tank DW**, **Bialek W.** Collective behavior of place and non-place neurons in the hippocampal network. *Neuron* 96: 1178–1191.e4, 2017. doi:10.1016/j.neuron.2017.10.027.
49. **Kapoor V**, **Urban NN.** Glomerulus-specific, long-latency activity in the olfactory bulb granule cell network. *J Neurosci* 26: 11709–11719, 2006. doi:10.1523/JNEUROSCI.3371-06.2006.
50. **Koulakov AA**, **Rinberg D.** Sparse incomplete representations: a potential role of olfactory granule cells. *Neuron* 72: 124–136, 2011. doi:10.1016/j.neuron.2011.07.031.
51. **Migliore M**, **Hines ML**, **McTavish TS**, **Shepherd GM.** Functional roles of distributed synaptic clusters in the mitral-granule cell network of the olfactory bulb. *Front Integr Neurosci* 4: 122, 2010. doi:10.3389/fnint.2010.00122.
52. **Liu S**, **Shao Z**, **Puche A**, **Wachowiak M**, **Rothermel M**, **Shipley MT.** Muscarinic receptors modulate dendrodendritic inhibitory synapses to sculpt glomerular output. *J Neurosci* 35: 5680–5692, 2015. doi:10.1523/JNEUROSCI.4953-14.2015.
53. **Schoppa NE**, **Kinzie JM**, **Sahara Y**, **Segerson TP**, **Westbrook GL.** Dendrodendritic inhibition in the olfactory bulb is driven by NMDA receptors. *J Neurosci* 18: 6790–6802, 1998. doi:10.1523/JNEUROSCI.18-17-06790.1998.
54. **Urban NN**, **Sakmann B.** Reciprocal intraglomerular excitation and intra- and interglomerular lateral inhibition between mouse olfactory bulb mitral cells. *J Physiol* 542: 355–367, 2002. doi:10.1113/jphysiol.2001.013491.
55. **Chen Z**, **Padmanabhan K.** Top-down control of inhibitory granule cells in the main olfactory bulb reshapes neural dynamics giving rise to a diversity of computations. *Front Comput Neurosci* 14: 59, 2020. doi:10.3389/fncom.2020.00059.
56. **Angelo K**, **Margrie TW.** Population diversity and function of hyperpolarization-activated current in olfactory bulb mitral cells. *Sci Rep* 1: 50, 2011. doi:10.1038/srep00050.
57. **Balu R**, **Strowbridge BW.** Opposing inward and outward conductances regulate rebound discharges in olfactory mitral cells. *J Neurophysiol* 97: 1959–1968, 2007. doi:10.1152/jn.01115.2006.
58. **Padmanabhan K**, **Urban NN.** Disrupting information coding via block of 4-AP-sensitive potassium channels. *J Neurophysiol* 112: 1054–1066, 2014. doi:10.1152/jn.00823.2013.
59. **Friedrich RW**, **Laurent G.** Dynamic optimization of odor representations by slow temporal patterning of mitral cell activity. *Science* 291: 889–894, 2001. doi:10.1126/science.291.5505.889.
60. **Padmanabhan K**, **Urban NN.** Intrinsic biophysical diversity decorrelates neuronal firing while increasing information content. *Nat Neurosci* 13: 1276–1282, 2010. doi:10.1038/nn.2630.
61. **Hallem EA**, **Carlson JR.** Coding of odors by a receptor repertoire. *Cell* 125: 143–160, 2006. doi:10.1016/j.cell.2006.01.050.
62. **Meister M**, **Bonhoeffer T.** Tuning and topography in an odor map on the rat olfactory bulb. *J Neurosci* 21: 1351–1360, 2001. doi:10.1523/JNEUROSCI.21-04-01351.2001.
63. **Rubin BD**, **Katz LC.** Optical imaging of odorant representations in the mammalian olfactory bulb. *Neuron* 23: 499–511, 1999. doi:10.1016/s0896-6273(00)80803-x.
64. **Saito H**, **Chi Q**, **Zhuang H**, **Matsunami H**, **Mainland JD.** Odor coding by a mammalian receptor repertoire. *Sci Signal* 2: ra9, 2009. doi:10.1126/scisignal.2000016.
65. **Soucy ER**, **Albeanu DF**, **Fantana AL**, **Murthy VN**, **Meister M.** Precision and diversity in an odor map on the olfactory bulb. *Nat Neurosci* 12: 210–220, 2009. doi:10.1038/nn.2262.
66. **Wachowiak M.** All in a sniff: olfaction as a model for active sensing. *Neuron* 71: 962–973, 2011. doi:10.1016/j.neuron.2011.08.030.
67. **Nguyen Chi V**, **Müller C**, **Wolfenstetter T**, **Yanovsky Y**, **Draguhn A**, **Tort ABL**, **Brankačk J.** Hippocampal respiration-driven rhythm distinct from theta oscillations in awake mice. *J Neurosci* 36: 162–177, 2016. doi:10.1523/JNEUROSCI.2848-15.2016.
68. **MacLean JN**, **Watson BO**, **Aaron GB**, **Yuste R.** Internal dynamics determine the cortical response to thalamic stimulation. *Neuron* 48: 811–823, 2005. doi:10.1016/j.neuron.2005.09.035.
69. **Bender DA**, **Ni R**, **Barbour DL.** Spontaneous activity is correlated with coding density in primary auditory cortex. *J Neurophysiol* 116: 2789–2798, 2016. doi:10.1152/jn.00474.2016.
70. **Stakic J**, **Suchanek JM**, **Ziegler GP**, **Griff ER.** The source of spontaneous activity in the main olfactory bulb of the rat. *PLoS One* 6: e23990, 2011. doi:10.1371/journal.pone.0023990.
71. **Thompson GJ**, **Sanganahalli BG**, **Baker KL**, **Herman P**, **Shepherd GM**, **Verhagen JV**, **Hyder F.** Spontaneous activity forms a foundation for odor-evoked activation maps in the rat olfactory bulb. *Neuroimage* 172: 586–596, 2018. doi:10.1016/j.neuroimage.2018.01.051.
72. **Carrillo-Reid L**, **Han S**, **Yang W**, **Akrouh A**, **Yuste R.** Controlling visually guided behavior by holographic recalling of cortical ensembles. *Cell* 178: 447–457.e5, 2019. doi:10.1016/j.cell.2019.05.045.
73. **Laurent G**, **Stopfer M**, **Friedrich RW**, **Rabinovich MI**, **Volkovskii A**, **Abarbanel HD.** Odor encoding as an active, dynamical process: experiments, computation, and theory. *Annu Rev Neurosci* 24: 263–297, 2001. doi:10.1146/annurev.neuro.24.1.263.
74. **Schneidman E.** Towards the design principles of neural population codes. *Curr Opin Neurobiol* 37: 133–140, 2016. doi:10.1016/j.conb.2016.03.001.
75. **Shlens J**, **Field GD**, **Gauthier JL**, **Grivich MI**, **Petrusca D**, **Sher A**, **Litke AM**, **Chichilnisky EJ.** The structure of multi-neuron firing patterns in primate retina. *J Neurosci* 26: 8254–8266, 2006. doi:10.1523/JNEUROSCI.1282-06.2006.
76. **Burton SD.** Inhibitory circuits of the mammalian main olfactory bulb. *J Neurophysiol* 118: 2034–2051, 2017. doi:10.1152/jn.00109.2017.
77. **Gilra A**, **Bhalla US.** Bulbar microcircuit model predicts connectivity and roles of interneurons in odor coding. *PLoS One* 10: e0098045, 2015. doi:10.1371/journal.pone.0098045.
78. **Willhite DC**, **Nguyen KT**, **Masurkar AV**, **Greer CA**, **Shepherd GM**, **Chen WR.** Viral tracing identifies distributed columnar organization in the olfactory bulb. *Proc Natl Acad Sci USA* 103: 12592–12597, 2006. doi:10.1073/pnas.0602032103.
79. **Petzold GC**, **Hagiwara A**, **Murthy VN.** Serotonergic modulation of odor input to the mammalian olfactory bulb. *Nat Neurosci* 12: 784–791, 2009. doi:10.1038/nn.2335.
80. **Rothermel M**, **Wachowiak M.** Functional imaging of cortical feedback projections to the olfactory bulb. *Front Neural Circuits* 8: 73, 2014. doi:10.3389/fncir.2014.00073.
81. **Tantirigama MLS**, **Huang HH-Y**, **Bekkers JM.** Spontaneous activity in the piriform cortex extends the dynamic range of cortical odor coding. *Proc Natl Acad Sci USA* 114: 2407–2412, 2017. doi:10.1073/pnas.1620939114.
82. **Kepecs A**, **Uchida N**, **Mainen ZF.** Rapid and precise control of sniffing during olfactory discrimination in rats. *J Neurophysiol* 98: 205–213, 2007. doi:10.1152/jn.00071.2007.
83. **Rinberg D**, **Koulakov A**, **Gelperin A.** Speed-accuracy tradeoff in olfaction. *Neuron* 51: 351–358, 2006. doi:10.1016/j.neuron.2006.07.013.
84. **Uchida N**, **Mainen ZF.** Speed and accuracy of olfactory discrimination in the rat. *Nat Neurosci* 6: 1224–1229, 2003. doi:10.1038/nn1142.